THE JOURNAL OF PHYSICAL CHEMISTRY B

ARTICLE

pubs.acs.org/JPCB

New Insights into the Substrate−Plasma Polymer Interface

Rodney T. Chen,[†,‡] Benjamin W. Muir,[*,‡] Lars Thomsen,[§] Anton Tadich,[§] Bruce C. C. Cowie,[§] Georgina K. Such,[†] Almar Postma,[†,‡] Keith M. McLean,[‡] and Frank Caruso[†]

[†]Department of Chemical and Biomolecular Engineering, The University of Melbourne, Parkville, Victoria 3010, Australia

[‡]CSIRO Materials Science and Engineering, Bayview Avenue, Clayton, Victoria 3168, Australia

[§]Australian Synchrotron, 800 Blackburn Road, Clayton, Victoria 3168, Australia

Supporting Information

ABSTRACT: We describe a new method to characterize the underside (substrate interface) of plasma polymer (PP) thin films via their simple delamination from a sodium chloride single crystal substrate. By depositing the PP film onto an ionic bonded surface such as a sodium chloride crystal, the PP films investigated were easily delaminated from the substrate. Two plasma polymer films deposited from 1-bromopropane (BrPP) and allylamine (AAPP) were used to exemplify this new technique. The top- and underside (substrate−plasma polymer interface) of the films were examined by X-ray photoelectron spectroscopy (XPS) and synchrotron-based near edge X-ray adsorption fine structure (NEXAFS) spectroscopy. The results demonstrate that both films exhibit heterogeneous film structures with their chemical composition and levels of unsaturated species. The underside of both the BrPP and the AAPP films exhibited higher concentrations of oxygen, while their topsides contained higher levels of unsaturated species. These results provide useful insights into the BrPP and AAPP film formation and the chemistry. The delamination technique provides a simple method to analyze the early stages of film chemistry for plasma polymer thin films. Furthermore, this approach opens new opportunities for additional studies on the mechanisms and fundamentals of plasma polymer thin film formation with various monomers.

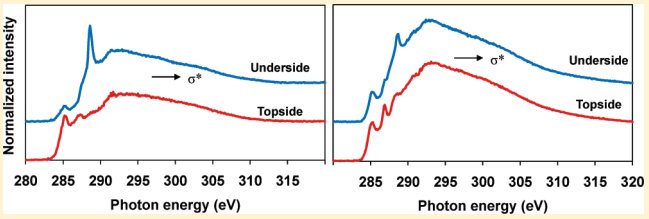

1. INTRODUCTION

During the past decade, there has been increasing interest in the use of plasma polymer (PP) thin films in applications as diverse as medical device coatings, optoelectronic materials, and protective barrier coatings on numerous devices.[1] A significant challenge in the development and optimization of PP thin films in these and other applications is the need to further the understanding of the complex plasma glow discharge processes that occur during their deposition. This is beneficial as it allows for a greater control over their physio-chemical properties.[2] Developing an accurate understanding of the activated plasma gaseous species−surface interface and the plasma physical chemistry during the glow discharge deposition of plasma polymer thin films has proven to be challenging because of the systems' complexity.[3] As such, plasma diagnostic tools[4] (e.g., mass and optical spectrometry, Langmuir probes, laser-induced fluorescence) are becoming increasingly valuable in this area but are problematic in the sense that during the glow discharge they can interact with the plasma and become contaminated with materials during deposition.[5] It is also experimentally difficult to discriminate between bulk plasma processes occurring throughout a glow discharge and those occurring near the plasma−substrate interface.[6]

It is known, but rarely reported, that the film chemistry and composition of a plasma polymer not only change when different substrates are used,[7] but that film composition and chemistry can vary significantly throughout a plasma polymer as it is deposited. This is due to a number of complex factors, including pressure change in the vacuum system as the monomer species are fragmented, the mode of power delivery (pulsed versus continuous wave), substrate effects, generation of reactive plasma species (which are monomer and system dependent), the rate of thin film deposition versus etching processes, the generation of vacuum ultraviolet radiation (VUV), and afterglow reactions.[8] The heterogeneity arising from a compositional gradient of plasma polymer chemistry and structure during deposition can have implications for the stability, adhesion, tribological, and optical properties of PP films in some applications.[9] Thus, the interfacial structure that exists between a PP and its substrate is of interest from both a practical and a fundamental point of view.[10]

Early work on this topic by Wrobel and Czeremuszkin[11] reported that PP thin films experience a vacuum UV dose depth profile, which increases from the surface to the substrate interface, resulting in different cross-link densities within the film. Yamaguchi and co-workers[12] found the presence of a transient interface layer in the initial growth stages of amorphous silicon

Received: January 26, 2011
Revised: April 12, 2011
Published: May 04, 2011

films using in situ ellipsometry. The refractive index of the transient layer was different from that of the bulk and was influenced by the substrate underlayer. This is in line with work by the groups Harata and co-workers and Short and co-workers, who also found that the substrate material onto which PP films are deposited can have an influence on its chemistry.[7]

The difficulty in analyzing the substrate−PP interface has led researchers to deposit ultrathin PP films (<10 nm) and characterize them using X-ray photoelectron and infrared spectroscopy[13] and recently with atomic force microscopy.[14] This allows for the chemical and morphological analysis of the film and the interface but is limited due to the fact that the top- and underside film chemistries are effectively "averaged" out. In light of this, chemical depth profiling of plasma polymers has been undertaken using ion etching, energy resolved XPS, Auger electron spectroscopy (AES), as well as X-ray and neutron reflectometry (XRR and NR).[15] A commonly used technique to perform thin film depth profile measurements in PP films is through the use of time-of-flight secondary ion mass spectroscopy (ToF-SIMs), which relies on the rastering of highly energetic ion species that bombard and etch away the thin film.[16] However, this technique can result in artifacts in the surface chemistry due to the etching process itself. There are very few reports on the direct analysis of the underside or substrate interface of PP films. One method that has been reported is via the selective backside etching of a PP film-coated silicon wafer with hydrofluoric acid.[17] This technique can also introduce artifacts in surface chemistry due to the oxidative etching process.[17c−e]

In this work, we report a method to analyze the underside of PP thin films, by depositing them on a sodium chloride (NaCl) single crystal substrate. Once a PP film is deposited, we have shown that we can exploit the film's poor adhesion to the salt crystal substrate via its delamination with double-sided tape to expose the underside. We exemplify this process with two different plasma polymers containing nitrogen and bromine functional groups, respectively. The use of aminated surfaces in biotechnology is widespread, and the plasma polymerization of amine monomers such as allylamine (AAPP) is an increasingly common route to such surfaces.[8e] Bromine plasma polymers are of interest as the surface bromine groups are available for nucleophilic substitution reactions commonly utilized in organic chemistry.[18] We have reported on the deposition of BrPP (from 1-bromopropane) as functional coatings for click chemistry on planar surfaces and recently as a route for fabricating reactive organic−inorganic Janus particles.[19] Chemical and structural analyses of the top- and underside surfaces of the BrPP and AAPP films were carried out using near X-ray photoelectron spectroscopy (XPS) and near edge X-ray absorption fine structure (NEXAFS) spectroscopy, which is applied for the first time on BrPP films. NEXAFS spectroscopy in Auger electron yield (AEY) mode has become a routine method for the surface analysis of organic thin films.[20] As the analysis depth of NEXAFS by AEY is similar to XPS, it is attractive to use these techniques in combination. A significant advantage of NEXAFS spectroscopy over XPS is its ability to distinguish different types of C−C unsaturated bonds. It can obtain molecule specific information by detecting the resonant excitations of electrons from core levels into unoccupied states through dipole interactions and their decay. The results obtained here from XPS and NEXAFS provide new insights into the chemistry and formation of these PP films and demonstrate the versatility of this delamination technique in analyzing the substrate−plasma polymer interface.

2. EXPERIMENTAL SECTION

2.1. Plasma Polymer Deposition. PP thin films were deposited onto a NaCl single crystal substrate (12.5 mm^2, 1 mm thick, SPI Supplies) via the radio frequency glow discharge (RFGD) of the monomers allylamine (Aldrich, 99%) and 1-bromopropane (Aldrich, 98%) in a custom built plasma reactor.[21] The plasma reactor consisted of two internal capacitively coupled copper electrodes housed in a cylindrical glass bell jar (height = 36 cm, diameter (d) = 18 cm). The electrodes are spaced 15 cm apart with the top electrode (d = 11 cm) connected to an RF power supply and the bottom electrode (d = 11 cm) grounded. The NaCl crystals were placed on the bottom electrode. A rotary pump kept the reactor under vacuum. A round-bottom flask containing the monomer was connected to the reactor chamber via a stainless steel line, and the flow of monomer vapor was controlled via a manual valve. The monomers were used as received and were degassed under vacuum prior to plasma deposition. Prior to plasma deposition, the reactor was evacuated to a base pressure of less than 0.1 Pa. The plasma deposition parameters were replicated from previous studies; a frequency of 175 and 200 kHz, a power of 20 W, an initial monomer pressure of 25 and 20 Pa, and a treatment time of 10 (final pressure 51 Pa) and 25 s (final pressure 41 Pa) were used for BrPP[18a] and AAPP,[10e] respectively. This resulted in films of approximately 35 nm in thickness (data not shown) on silicon wafers. Thicker films (ca. 70 nm on silicon wafers) were also deposited on the salt crystal substrate by increasing the deposition time to 30 (final pressure 59 Pa) and 100 s (final pressure 28 Pa) for the BrPP and AAPP, respectively. After the desired deposition time had been reached, the RF source was switched off, the monomer flow was stopped, and the reactor was immediately pumped down to base pressure before venting.

2.2. Plasma Polymer Delamination Procedure. Conductive double-sided carbon adhesive tape (SPI Supplies) was stuck onto small thin sheets of copper (0.5 × 1 mm). This allowed the tape to be easily handled and analyzed under XPS and NEXAFS spectroscopy. The tape was lightly and briefly applied onto a section of freshly deposited PP films on the NaCl substrate. The tape was then removed, inverting and exposing the underside of the PP section. After removing the tape, there was a demarcation from the delaminated section on the PP- coated salt crystal substrate. Complete delamination was confirmed with XPS analysis of the delaminated section being almost identical to the bare NaCl substrate (see the Supporing Information).

2.3. X-ray Photoelectron Spectroscopy. XPS analysis was performed on an AXIS HSi spectrometer (Kratos Analytical Ltd., UK) equipped with a monochromated $Al_{K\alpha}$ X-ray source at a power of 144 W (12 mA, 12 kV). Three different positions per sample were analyzed, with atomic concentrations of each element calculated by integration of the area of the relevant peaks and by applying sensitivity factors supplied by the manufacturer. Peak assignments were determined from the measured binding energy values that were charge corrected with respect to the main aliphatic hydrocarbon C 1s core level peak, which was set at 285.2 eV.[22] Survey spectra were acquired at a pass energy of 320 eV, from which all elements were identified. High-resolution C 1s spectra were also obtained at a pass energy of 40 eV and quantified using a minimization algorithm to calculate optimized curve-fits and determine the relative contributions from specified functional groups.

2.4. Near Edge X-ray Absorption Fine Structure (NEXAFS) Spectroscopy. NEXAFS measurements were carried out on the

soft X-ray beamline (SXR, 14-ID) at the Australian Synchrotron.[23] Samples were loaded into a UHV chamber, where a vacuum of 2×10^{-10} mbar was maintained. The beamline is equipped with an Apple II undulator, adjusted to produce horizontally polarized soft X-rays, which are then passed through a monochromator (Peterson plane grating, 1200 lines mm^{-1}). The photon flux on the beamline ranged from $1-3 \times 10^{11}$ photons/s/200 mA with an energy of 550 eV, and the photon spot size on the sample was approximately 0.6×0.6 mm. To compensate for sample charging, all spectra were acquired with a flood gun turned on. Thus, NEXAFS spectra from the carbon, oxygen, and nitrogen K-edge were acquired in Auger electron yield (AEY) mode with the beam at 90° with respect to the sample surface. The photon energy range for carbon, oxygen, and nitrogen was 270−320, 520−560, and 390−430 eV, respectively, with a step size of 0.1 eV. No radiation damage to the films was observed following repeated exposure from the light (this was seen by recording multiple spectra at the same spot on the films, which retained the same spectral features). Each NEXAFS spectrum was normalized to the incident photon flux by measuring, in parallel, the drain current (I_0) from a fine gold mesh placed just before the sample. To account for any intrinsic carbon, nitrogen, and oxygen contamination of the reference mesh, NEXAFS spectra from a photodiode were obtained and used to further normalize the data, following the method by Watts et al.[24]

3. RESULTS AND DISCUSSION

In this work, we exploit the poor adhesion of PP films on a NaCl single crystal substrate to expose its underside via simple and straightforward delamination using double-sided tape (Scheme 1). The underside of the PP films was directly analyzed with XPS and NEXAFS spectroscopy, and the structural and chemical composition was compared to the topside.

3.1. XPS Analysis. The elemental composition, as determined from analysis of the XPS survey spectra of the PP films, shows that there are some marked differences between the top- and underside (Figure 1). Sodium and chlorine were not detected on the topside of either film, and the shape of the spectral intensity background did not show any effects from the underlying salt crystal substrate, indicating a film thickness significantly greater than 10 nm. The chemical compositions on the topside of both PP films on the salt crystal substrate and silicon wafer (XPS data not shown) were within 10% of each other. For the underside of both films, low levels of silicon (from the CDST), sodium, and chlorine (from the salt crystal substrate) were detected. In the case of the 35 nm films, the concentration of bromine in the underside of the BrPP film was much lower than that of the topside (8.9% vs 17.1%) in contrast to the AAPP film, where both sides had a very similar concentration of nitrogen (12.3% vs 12.5%). The 70 nm AAPP exhibited a similar pattern (both sides with 12.3% nitrogen). In the case of the 70 nm BrPP film, the chemical heterogeneity was less pronounced with the underside containing concentrations of bromine similar to those of the underside of the 35 nm film at 8.3%, but there was a significantly lower concentration of bromine (7.0%) on the topside. This suggests that the longer plasma deposition time led to a more chemically homogeneous BrPP film, with minimal impact upon film chemistry in the case of the AAPP film. In both the BrPP and the AAPP films, the disparity in the oxygen and carbon content on the top- and underside remained fairly similar irrespective of

Scheme 1. Schematic Illustration of the Procedure Used To Expose the Underside of PP Thin Film by Its Delamination from a NaCl Single Crystal Using Conductive Double-Sided Tape (CDST)

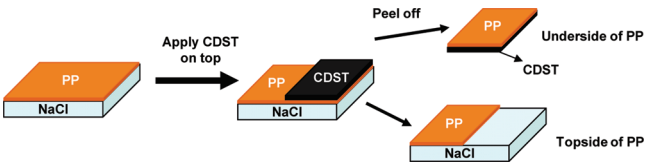

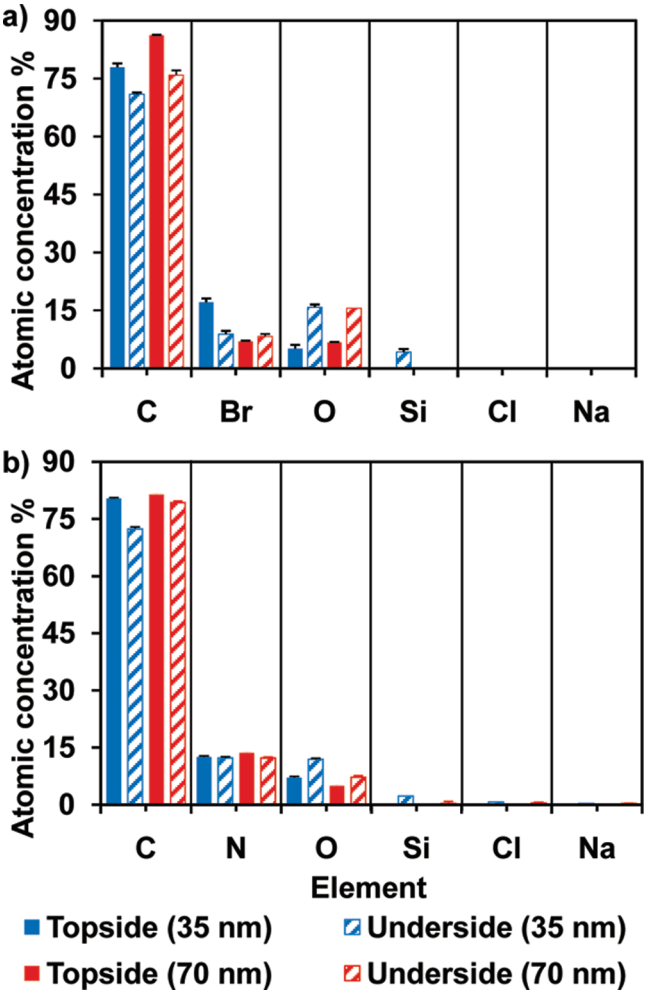

Figure 1. Elemental composition as determined by XPS of the top- and underside of 35 and 70 nm (a) BrPP and (b) AAPP films. The data represent averages from three different sample points of each sample.

film thickness, albeit somewhat less pronounced in the case of the 70 nm AAPP film.

Figure 1 also shows that for all films, the underside when compared to the topside contains a considerably greater concentration of oxygen and conversely a lower concentration of carbon. The oxygen to carbon ratio (O/C) on the top- and underside of the 35 nm BrPP film was 0.06 and 0.22, respectively. For the 70 nm BrPP film, the ratios were 0.08 and 0.21, respectively. In 35 nm AAPP film, the ratios of the top- and underside were 0.09 and 0.16, respectively. With the 70 nm AAPP film, both ratios were the same at 0.06. Neither monomer

dx.doi.org/10.1021/jp200864k |J. Phys. Chem. B 2011, 115, 6495–6502

contains oxygen; hence, the oxygen content in the films may be due to postoxidation reactions with ambient atmosphere and possibly to a small extent from residual oxygen gas in the vacuum system during plasma polymerization. Carpick and co-workers also observed higher oxygen content in the underside of plasma deposited diamond thin films on seeded silicon wafers, which was acid etched to form free-standing films. They attributed the increase in oxygen to postoxidation reactions with ambient atmosphere, the seeding process, the oxide substrate, as well as the acid etching process. In our case, we rationalize the discrepancy in the chemical composition of the top- and underside of the BrPP and AAPP films to the differing reactions with radical species within the film. It is well-known that within many PP films, stable and long-lived radicals can be created.[25] No efforts were made to minimize the concentration of trapped radicals, such as leaving the samples under vacuum for extended periods of time or allowing the continual flow of monomer vapor after the plasma was extinguished. However, it is hypothesized that when the plasma is extinguished, any surface radicals on the topside of the PP films would readily react with any residual gaseous monomer species inside the plasma reactor.[18c] In the case of BrPP, the surface halogenation reactions that may be occurring in this process include hydrogen abstraction and insertion into C−H bonds from bromine radicals and reactions of radical centers in the PP thin film with gaseous bromine molecules, resulting in more bromine on the topside.[26] Another possible reaction occurring during the bromination of the BrPP thin film is via the addition of bromine to C═C bonds, resulting in the formation of −CHBr−CHBr− moieties. The radicals in the underside of the BrPP would be significantly less available for participation in the halogenation reactions described and therefore less able to incorporate additional bromine species. Hence, once the film is delaminated from the salt crystal substrate, the reaction of oxygen species from the ambient air with radical species on the underside of the PP film would occur to a greater extent when compared to the topside. This is due to the fact that the topside radicals have already been "quenched" significantly through the various halogenation reaction pathways described, resulting in more oxygen in the underside of the BrPP. As mentioned earlier, there is a significant variation in the film chemistry in terms of the difference in bromine concentration between the topsides of the 35 and 70 nm films. Increasing the deposition time causes a greater level of fragmentation of the 1-bromopropane monomer as evidenced by the increase in pressure, by 26 Pa, in the plasma reactor during plasma deposition of the 35 nm film, and by 34 Pa, in the case of the 70 nm film. This increase in pressure and, therefore, increase in monomer fragmentation appears to lead to a loss in bromine on the topside of the 70 nm film when compared to the 35 nm film.

In the case of AAPP, where the concentrations of nitrogen in both sides of the film were similar, quenching of residual radicals on the topside of AAPP might occur to a much lesser extent as compared to the BrPP. We hypothesize that residual gaseous vapors of allylamine may not readily polymerize by radical addition through its vinyl group for two reasons. First, the termination of the growing radical chain ends by hydrogen abstraction is more effective, and, second, the stability of the allylic radical itself would not propagate polymerization effectively.[2b,27] It has been suggested that allylamine monomer undergoes limited fragmentation and radical production and the plasma-gas-phase species are rather insensitive to the plasma load power.[2b,27] Hence, there is extensive oligomerization,

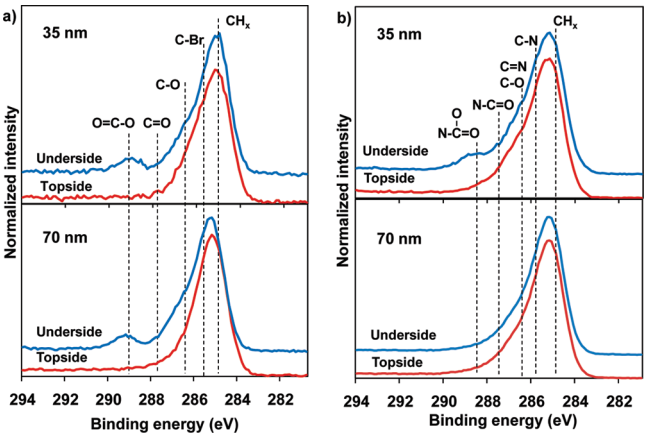

Figure 2. High-resolution C 1s XPS spectra of the top- and underside of (a) BrPP and (b) AAPP films. Dotted lines roughly represent expected peaks arising from different functional groups.

with the primary mechanism of film formation arising from plasma-induced reactions of intact allylamine molecules with surface radicals.[2b,e,27] Previous reports on the AFM analysis of AAPP films have shown that they are generally very smooth, which indicates that film growth occurs via a layer-by-layer mechanism (Frank−van der Merwe).[2e,14] This translates to a more even bulk distribution of nitrogen species and fewer residual radicals in the AAPP film, which reduces the extent of postoxidation reactions occurring. This may also explain the lack of significant variation in the film chemistry between the 35 and 70 nm AAPP film in contrast to the BrPP films (Figure 1).

Differences in film chemistry can also be seen in the high-resolution C 1s spectra between the top- and underside of the 35 nm films (Figure 2). The main difference in both films is an extra component around 289 eV in the underside as compared to the topside spectra. This component is attributable to acid, ester, and amide functionalities. This increase in oxygen bonded carbon species correlates well with the elemental data from the XPS survey spectra. Assignment of the C 1s peak components in the spectra based on chemical shifts alone is difficult due to the closeness in binding energies of C−O and C−Br bonds, as well as interfering contributions from the secondary shifts arising from O═C−O species.[22,28] The profiles of the C 1s spectra from 70 nm films did not display significant variations when compared to the 35 nm films. In the BrPPs, the C 1s spectra of the undersides were very similar for both thicknesses (Figure 2a). In the case of the topsides, there is a slight difference, with the 70 nm film displaying a narrower C 1s peak. This is indicative of a more "hydrocarbon like" film, which correlates with the data from Figure 1, with the higher carbon and lower bromine content in the topside of the 70 nm film. With the AAPP films, the only detectable difference is in the underside spectra of the 70 nm film where there is an absence of a peak around 288−289 eV (Figure 2b). Again, this correlates with the data from Figure 1, showing the lower oxygen content in the underside of the 70 nm AAPP film.

As mentioned earlier, low levels of silicon were detected in the underside of the films. However, from analysis of the high-resolution C 1s spectrum, there were no components arising from C−Si bonds, which occur at ca. 283 eV.[29] Hence, the source of the silicon is most certainly due to migration of adventitious low molecular weight polysiloxanes arising from the adhesive

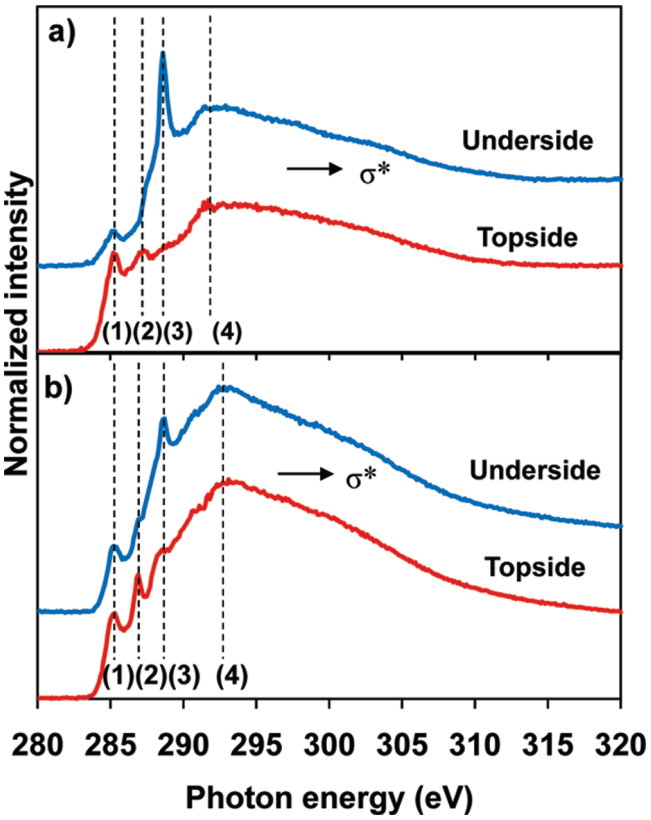

Figure 3. C 1s K-edge AEY NEXAFS spectra of top- and underside of 35 nm (a) BrPP (b) AAPP films. All spectra are normalized in height between the pre- and post-edge. Dotted lines represent resonant peak positions.

Table 1. C 1s K-Edge Peak Positions and Assignments for BrPP and AAPP[31] from Figure 3

line	BrPP position (eV)	assignment
1	285.2	C═C π^*
2	287.3	C−H σ^*
3	288.6	C═O σ^*
4	292.7	C−C, C−O σ^*
line	**AAPP position (eV)**	**assignment**
1	285.2	C═C π^*
2	286.9	C≡N π^*
3	288.6	C═O σ^* (amide)
4	293.1	C−C, C−N σ^*

tape (as verified by XPS survey spectra; see the Supporting Information). This is supported by the fact that significantly less silicon was detected on the undersides of the thicker deposits of both films. With further optimization of this technique and careful choice of the adhesive materials used to delaminate the PP from the NaCl substrate, such effects of contamination could be negated.

3.2. NEXAFS Analysis. To further analyze the chemistry across the 35 nm BrPP and AAPP films and detect any molecular orientation of terminal chains and characterize the various resonances occurring from unsaturated species, C 1s, O 1s, and N 1s K-edge AEY NEXAFS spectroscopy was performed. Figure 3 shows the AEY C 1s K-edge NEXAFS spectra from the top- and underside of the BrPP and AAPP films, which clearly demonstrate the heterogeneous nature of the films. In Figure 3a, the C 1s K-edge spectra from the BrPP film clearly confirm the presence of unsaturated carbon species arising from intense energy peaks at 285.2 eV, which is typical of C 1s → π^* (C═C) transitions. This shows the greater surface sensitivity of this technique as compared to XPS, as $\pi-\pi^*$ shake-up features around 292 eV were not present on either surface of the BrPP film in the C 1s XPS spectra (Figure 2). Table 1 summaries the other resonances observed in the spectra, which include C 1s → σ^*(C−H) at 287.3 eV, C 1s → π^*(C═O) resonance at 288.6 eV, and finally a broader C 1s → σ^*(C−C; C−O) resonance feature above 292.7 eV.[30] Because of the multiphoton resonance absorptions and the broader nature of the higher energy σ-bonded species, only the lower energy features will be compared and discussed. In comparing the observed resonances of the top- and underside, it is clear that there are significant differences in their intensities, size, and energies. While AEY NEXAFS is not a quantitative technique, it is clear that the topside is considerably more unsaturated than the underside due to the greater contribution of C 1s → π^* resonances at 285.2 eV. This result is to be expected as the pressure rises by 27 Pa during the course of the plasma polymerization process, as more gaseous plasma species are fragmented. This may result in the generation of more unsaturated species in the outermost regions of the plasma polymer film. As the 1-bromopropane monomer is saturated, the fragmentation and recombination processes occurring during plasma polymerization will involve the formation of free radicals via hydrogen and bromine abstraction. This will lead to the formation of a certain amount of unsaturated species within the plasma polymer film.[31] It is clear that the underside of the BrPP has significantly more contributions from resonances due to carbon and oxygen bonds such as the sharp C 1s → π^*(C═O) resonance at 288.6 eV. This result is to be expected due to the fact it has a greater oxygen content and contains additional O−C═O chemical species, as observed from XPS analysis (Figures 1 and 2). We also tested for possible orientation of polymer chains in the top- and underside of the BrPP film by analyzing C 1s K-edge NEXAFS spectra using both horizontally and vertically polarized light. No difference was seen in the spectra obtained from horizontally or vertically polarized light, indicating no preferred orientation, presumably due to the amorphous and cross-linked nature of the plasma polymer films.

In Figure 3b, the C 1s K-edge spectra from the AAPP film also show the presence of unsaturated carbon species, with the topside having greater contributions at 285.2 and 286.9 eV, which are typical of transitions to π^* orbitals from C 1s → π^* and C≡N resonances, respectively.[32] The presence of nitriles is expected in the AAPP film, as we deposited it using a load power of 20 W. The concentration of nitrile species has been found to diminish with decreasing plasma load powers.[20c,32] There is an absence of a resonant peak at 285.9 eV, which corresponds to π^* orbital transitions from C═N bonds, in the spectrum from both sides, an observation that was also reported by Shard et al.[32] While the topside has a shoulder at 288.6 eV, the underside has a distinct peak that corresponds to carbonyl species most likely from amide groups. This correlates well with the higher oxygen

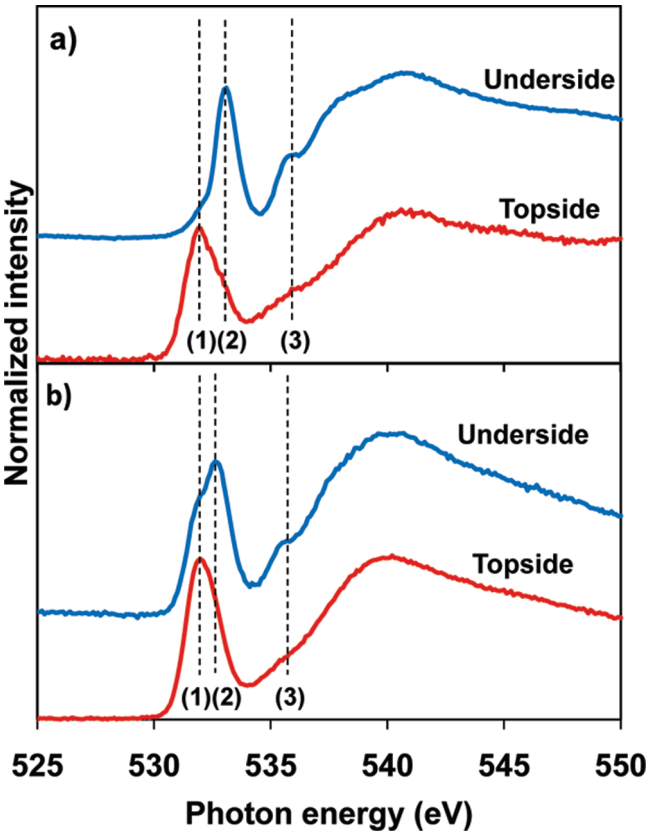

Figure 4. O 1s K-edge AEY NEXAFS spectra of top- and underside of 35 nm (a) BrPP and (b) AAPP films. All spectra are normalized in height between the pre- and post-edge. Dotted lines represent resonant peak positions.

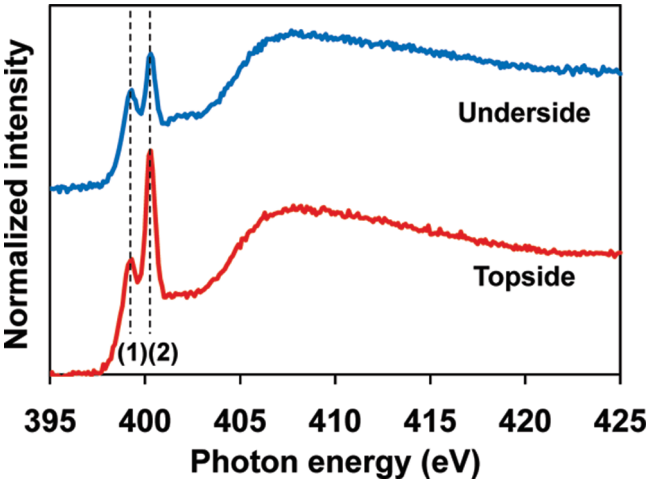

Figure 5. N 1s K-edge AEY NEXAFS spectra of top- and underside of 35 nm AAPP films. Spectra are normalized in height between the pre- and post-edge. Dotted lines represent resonant peak positions.

content and the presence of amide species obtained from the XPS analysis of the underside.

Figure 4 shows the AEY O 1s K-edge NEXAFS spectra for the top- and underside of the BrPP and AAPP films. Both films contain unsaturated species with resonances between 532 and 533 eV arising from O 1s → π^* (C═O) transitions along with dominant O 1s → σ^* (C−O, C═O) transitions appearing at ca. 540 eV.[30a,33] The π^* resonances for the BrPP are quite distinct with the transitions occurring predominately from acetate (531.9 eV, line 1) and carbonate (532 eV, line 2) groups for the top and underside, respectively. A clear distinction in the underside of both films as compared to their topside is the presence of a shoulder around 536 eV (line 3). This shoulder is representative of a second O 1s (O−R) → π^* (C═O) transition arising from the delocalization of the π^* (C═O) transition onto the −OR oxygen site. This occurs for species with two chemically nonequivalent sites such as ester and anhydride groups.[33,34] This second transition is absent from amide, aldehyde, and ketone groups and therefore indicates the underside of the PP films contain different oxygen functionalities, including ester and anhydride species, when compared to the topside of the films. This also correlates well with the data from the high-resolution C 1s XPS spectra (Figure 2).

Figure 5 shows the AEY N 1s K-edge NEXAFS spectra for the top- and underside of the 35 nm AAPP film. The spectra display two sharp resonant π^* features at peaks at 399.3 eV (1) and 400.3 eV (2) along with a broad N 1s → σ^* (C−N) resonance around 407 eV. As seen with the C 1s K-edge, the topside exhibits greater contributions from resonant π^* features when compared to the underside. This is yet another indication that the topside is more unsaturated than the underside. In the underside, just after the resonance at 400.3 eV, there is a weak resonance at 401.4 eV that may be assigned to the N 1s → σ^* (N−H) transition.[31] Previous studies have reported π^* resonances from 399.1 eV and below and assigned them to C═N bonds.[32,35] This suggests that the peak at 399.3 eV may arise from imine species. However, in the C 1s K-edge, peaks arising from C═N bonds (ca. 285.5−285.9 eV) were absent. The peak at 400.3 eV can be assigned to C≡N bonds, as it was present in the C 1s K-edge spectra. It has been suggested that due to conjugation, nitrile species may contribute to additional transitions at lower energies. Parent et al. investigated acrylonitrile multilayers and reported a π^* resonance with a −0.9 eV energy shift from the main nitrile peak.[36] It was reported that this is due to conjugation of C═C groups with C≡N groups. As was first observed by Shard et al.[32] and others,[20c,f] it is clear from the XPS and NEXAFS data that during plasma deposition of allylamine, there are chemical transformations occurring to the amine group, which results in the generation of PP film chemistries that contain multiple bonds between carbon and nitrogen. Additionally, these unsaturated CN species occur in greater concentrations on the topside of the film as compared to the underside. As the AAPP film studied in this work was deposited with a relatively high plasma load power, the formation of unsaturated CN species is not surprising, and this has been rationalized by various groups as arising from an imine intermediate.[2e,20c,32] This imine intermediate may have an indirect contribution to the resonance observed at 399.3 eV, resulting in one of the π^* resonances shifting to lower photon energies from the main nitrile peak. The data presented here, which show that the 35 nm AAPP contains a higher concentration of unsaturated species at the topside compared to the underside, are in good agreement with this suggested mechanism.

The N 1s K-edge spectra of our AAPP films are somewhat different from those reported by Oran et al.[20c] This may be the result of a number of factors, including the fact that the plasma polymer films were deposited on different substrates and that different deposition methods (continuous wave versus pulsed plasma) were used, which are known to produce significantly

different surface chemistries.[2f,8b] Second, the spectra acquired by Oran et al.[20c] were measured in total electron yield (TEY) mode with the beam at 55° to the sample surface, and our spectra were acquired in Auger electron yield (AEY) mode with the beam at 90° to the sample surface, which will result in different spectra being obtained. This difference in acquisitions angle will affect the relative intensities of the π^* and σ^* resonances captured here in comparison to the data presented by Oran et al.[20c] In a separate study by Shard et al.,[32a] the N 1s K-edge spectra of the AAPP films, which were also deposited in a continuous wave plasma polymerization, were similar to those reported here, with the only significant difference being the fact that our π^* component is split in two.

4. CONCLUSIONS

We have presented a novel method to expose and directly analyze the underside of a PP thin film via delamination from an ionic bonded substrate without the need for acid etching. We have exemplified this via the use of plasma polymers with bromine and nitrogen functional groups. Analysis from XPS and NEXAFS spectroscopy reveals that the chemical composition and molecular orientation of the top- and underside of BrPP and AAPP films can be heterogeneous in nature, and this has led to insights into the formation and residual chemistries of the film interface. The differences in the level of unsaturation and the bromine and oxygen content in the top- and underside of the BrPP films highlight the changes in the plasma glow discharge during the course of the thin film depositions and suggest that halogenation reactions occur in the afterglow. This was observed by the extent of postdeposition oxidation reactions of long-lived radicals after exposure to ambient atmosphere of the top- and underside of the BrPP film. In the case of the AAPP deposited films, there was less variation in chemical composition between the top- and underside in comparison to the BrPP, as determined by XPS. However, with NEXAFS analysis, it was observed that there also was a greater level of unsaturation in the topside, and this is attributable to the increasing formation of nitrile species from imine intermediates. It is acknowledged that PP depositions on an ionically bonded substrate represent an exceptional case when compared to other commonly used substrates such as polymers, metals, and semiconductors. The substrate effects[7] of the salt crystal on the initial PP film chemistry could well be different from these other substrates, where the PP film is often covalently attached. However, from the XPS and NEXAFS results, the PP films on the salt crystal substrate exhibited characteristics similar to those deposited on silicon wafers and importantly correlate well with previous reports. Further work is required to ascertain the applicability of other plasma polymer systems and the films obtained using the salt crystal substrate. The development of this technique to further probe the chemistry of PP films during the early stages of film formation at the substrate interface should provide valuable insights into the properties of early stage formation of PP films.

■ ASSOCIATED CONTENT

Supporting Information. XPS analysis of the NaCl crystal substrate, along with XPS and NEXAFS analysis of the conductive double-sided tape (CDST). This material is available free of charge via the Internet at http://pubs.acs.org.

■ AUTHOR INFORMATION

Corresponding Author
*E-mail: ben.muir@csiro.au.

■ ACKNOWLEDGMENT

Part of this research was undertaken on the soft X-ray beamline at the Australian Synchrotron, Victoria, Australia, and was supported by the Australian Research Council (F.C. Discovery Project and Federation Fellowship). R.T.C. gratefully acknowledges the CSIRO OCE for provision of a studentship.

■ REFERENCES

(1) (a) Weikart, C. M.; Matsuzawa, Y.; Winterton, L.; Yasuda, H. K. *J. Biomed. Mater. Res., Part A* **2001**, *54*, 597. (b) Deshpande, P.; Notara, M.; Bullett, N.; Daniels, J. T.; Haddow, D. B.; MacNeil, S. *Tissue Eng., Part A* **2009**, *15*, 2889–2902. (c) Hu, X.; Zhao, X.; Uddin, A.; Lee, C. B. *Thin Solid Films* **2005**, *477*, 81–87. (d) Huang, C.; Yu, Q. *J. Appl. Polym. Sci.* **2010**, *116*, 245–251. (e) Zheludkevich, M. L.; Serra, R.; Grundmeier, G.; Yang, L. H.; Ferreira, M. G. S. *Surf. Coat. Technol.* **2006**, *200*, 4040–4049.

(2) (a) Toole, L.; Short, R. D. *J. Chem. Soc., Faraday Trans.* **1997**, 93. (b) Beck, A. J.; Candan, S.; Short, R. D.; Goodyear, A.; Braithwaite, N. S. J. *J. Phys. Chem. B* **2001**, *105*, 5730–5736. (c) Zhang, J.; Feng, X.; Xie, H.; Shi, Y.; Pu, T.; Guo, Y. *Thin Solid Films* **2003**, *435*, 108–115. (d) Hallil, A.; Despax, B. *Thin Solid Films* **2000**, *358*, 30–39. (e) Choukourov, A.; Biederman, H.; Slavinska, D.; Hanley, L.; Grinevich, A.; Boldyryeva, H.; Mackova, A. *J. Phys. Chem. B* **2005**, *109*, 23086–23095. (f) Denis, L.; Cossement, D.; Godfroid, T.; Renaux, F.; Bittencourt, C.; Snyders, R.; Hecq, M. *Plasma Processes Polym.* **2009**, *6*, 199–208. (g) Milella, A.; Palumbo, F.; Favia, P.; Cicala, G.; d'Agostino, R. *Pure Appl. Chem.* **2005**, *77*, 399. (h) Unger, W. E. S.; Swaraj, S.; Oran, U.; Lippitz, A. *Surf. Interface Anal.* **2006**, *38*, 522–525.

(3) (a) Steen, M. L.; Butoi, C. I.; Fisher, E. R. *Langmuir* **2001**, *17*, 8156–8166. (b) Guerin, D. C.; Hinshelwood, D. D.; Monolache, S.; Denes, F. S.; Shamamian, V. A. *Langmuir* **2002**, *18*, 4118–4123. (c) Denis, L.; Cossement, D.; Godfroid, T.; Renaux, F.; Bittencourt, C.; Snyders, R.; Hecq, M. *Plasma Processes Polym.* **2009**, *6*, 199–208.

(4) (a) Stillahn, J. M.; Trevino, K. J.; Fisher, E. R. *Annu. Rev. Anal. Chem.* **2008**, *1*, 261. (b) Fisher, E. R. *Plasma Processes Polym.* **2004**, *1*, 13–27. (c) Barton, D.; Bradley, J. W.; Steele, D. A.; Short, R. D. *J. Phys. Chem. B* **1999**, *103*, 4423–4430. (d) Guerin, D. C.; Fernsler, R. F.; Shamamian, V. A. *J. Vac. Sci. Technol., A* **2003**, *21*, 1724–1733. (e) Hong, J.; Truica-Marasescu, F.; Martinu, L.; Wertheimer, M. R. *Plasma Polym.* **2002**, *7*, 245–260.

(5) Hopkins, M. B. *J. Res. Natl. Inst. Stand. Technol.* **1995**, *100*, 415.

(6) (a) Wheale, S. H.; Barker, C. P.; Badyal, J. P. S. *Langmuir* **1998**, *14*, 6699–6704. (b) Bogaerts, A.; Bultinck, E.; Eckert, M.; Georgieva, V.; Mao, M.; Neyts, E.; Schwaederlé, L. *Plasma Processes Polym.* **2009**, *6*, 295–307.

(7) (a) Furuya, K.; Nakanishi, R.; Okumura, H.; Makita, M.; Harata, A. *Thin Solid Films* **2008**, *516*, 6028–6032. (b) Vasilev, K.; Michelmore, A.; Griesser, H. J.; Short, R. D. *Chem. Commun.* **2009**, 3600. (c) Vasilev, K.; Michelmore, A.; Martinek, P.; Chan, J.; Sah, V.; Griesser, H. J.; Short, R. D. *Plasma Processes Polym.* **2010**, *7*, 824–835.

(8) (a) Holländer, A.; Kröpke, S.; Pippig, F. *Surf. Interface Anal.* **2008**, *40*, 379–385. (b) Förch, R.; Zhang, Z.; Knoll, W. *Plasma Processes Polym.* **2005**, *2*, 351–372. (c) Moisan, M.; Wertheimer, M. R. *Surf. Coat. Technol.* **1993**, *59*, 1–13. (d) Yasuda, H.; Hsu, T. *J. Polym. Sci., Part A: Polym. Chem.* **1977**, *15*, 81–97. (e) Siow, K. S.; Britcher, L.; Kumar, S.; Griesser, H. J. *Plasma Processes Polym.* **2006**, *3*, 392–418.

(9) (a) Shi, F. F. *Surf. Coat. Technol.* **1996**, *82*, 1–15. (b) Biederman, H.; Slavínská, D. *Surf. Coat. Technol.* **2000**, *125*, 371–376.

(10) (a) Bucknall, D. G. *Prog. Mater. Sci.* **2004**, *49*, 713–786. (b) Grundmeier, G.; Stratmann, M. *Annu. Rev. Mater. Res.* **2005**, *35*, 571–615. (c) Awaja, F.; Gilbert, M.; Kelly, G.; Fox, B.; Pigram, P. J.

Prog. Polym. Sci. **2009**, *34*, 948–968. (d) Muir, B. W.; Thissen, H.; Simon, G. P.; Murphy, P. J.; Griesser, H. J. *Thin Solid Films* **2006**, 500. (e) Muir, B. W.; Nelson, A.; Fairbrother, A.; Fong, C.; Hartley, P. G.; James, M.; McLean, K. M. *Plasma Processes Polym.* **2007**, *4*, 433–444.

(11) Wróbel, A. M.; Czeremuszkin, G. *Thin Solid Films* **1992**, *216*, 203–210.

(12) (a) Hatanaka, Y.; Ohkuwa, M.; Yamaguchi, T. *Appl. Surf. Sci.* **1993**, *65*−*66*, 507–510. (b) Hatanaka, Y.; Mitsuoka, K.; Yamaguchi, T. *Appl. Surf. Sci.* **1989**, *41*−*42*, 591–597.

(13) (a) Grundmeier, G.; Stratmann, M. *Thin Solid Films* **1999**, *352*, 119–127. (b) Alexander, M. R.; Payan, S.; Duc, T. M. *Surf. Interface Anal.* **1998**, *26*, 961–973. (c) Turner, R. H.; Boerio, F. J. *J. Adhes.* **2002**, *78*, 465–493. (d) Turner, R. H.; Boerio, F. J. *J. Adhes.* **2002**, *78*, 447–464. (e) Rosales, P. I.; Boerio, F. J. *J. Adhes.* **2007**, *83*, 267–287. (f) Wapner, K.; Grundmeier, G. *Surf. Coat. Technol.* **2005**, *200*, 100–103.

(14) Michelmore, A.; Martinek, P.; Sah, V.; Short, R. D.; Vasilev, K. *Plasma Processes Polym.* **2011**, DOI: 10.1002/ppap.201000140.

(15) (a) Scott, P.; Wieliczka, D.; Kruger, M. *Plasma Chem. Plasma Process.* **2009**, *29*, 559–566. (b) Girard-Lauriault, P.-L.; Retzko, I.; Swaraj, S.; Matsubayashi, N.; Gross, T.; Mix, R.; Unger, W. E. S. *Plasma Processes Polym.* **2010**, *7*, 474–481. (c) Sabata, A.; van Ooij, W. J.; Yasuda, H. K. *Surf. Interface Anal.* **1993**, *20*, 845–859. (d) Kim, H.; Foster, M. D.; Jiang, H.; Tullis, S.; Bunning, T. J.; Majkrzak, C. F. *Polymer* **2004**, *45*, 3175–3184. (e) Dennler, G.; Houdayer, A.; Raynaud, P.; Séguy, I.; Ségui, Y.; Wertheimer, M. R. *Plasma Polym.* **2003**, *8*, 43–59. (f) Unger, W. E. S.; Lippitz, A.; Wöll, C.; Heckmann, W. *Fresenius' J. Anal. Chem.* **1997**, *358*, 89–92.

(16) (a) Brison, J.; Muramoto, S.; Castner, D. G. *J. Phys. Chem. C* **2010**, *114*, 5565–5573. (b) Batan, A.; Mine, N.; Douhard, B.; Brusciotti, F.; De Graeve, I.; Vereecken, J.; Wenkin, M.; Piens, M.; Terryn, H.; Pireaux, J. J.; *Chem. Phys. Lett.* **2010**, *493*, 107–112.

(17) (a) Grundmeier, G.; Thiemann, P.; Carpentier, J.; Barranco, V. *Thin Solid Films* **2004**, *174*−*175*, 996–1001. (b) Oosterbaan, W. D.; Bolsee, J. C.; Gadisa, A.; Vrindts, V.; Bertho, S.; D'Haen, J.; Cleij, T. J.; Lutsen, L.; McNeill, C. R.; Thomsen, L.; *Adv. Funct. Mater.* **2010**, *20*, 792–802. (c) Sumant, A. V.; Grierson, D. S.; Gerbi, J. E.; Birrell, J.; Lanke, U. D.; Auciello, O.; Carlisle, J. A.; Carpick, R. W. *Adv. Mater.* **2005**, *17*, 1039–1045. (d) Sumant, A. V.; Gilbert, P. U. P. A.; Grierson, D. S.; Konicek, A. R.; Abrecht, M.; Butler, J. E.; Feygelson, T.; Rotter, S. S.; Carpick, R. W. *Diamond Relat. Mater.* **2007**, *16*, 718–724. (e) Sumant, A. V.; Grierson, D. S.; Gerbi, J. E.; Carlisle, J. A.; Auciello, O.; Carpick, R. W. *Phys. Rev. B* **2007**, *76*, 235429.

(18) (a) McGettrick, J. D.; Crockford, T.; Schofield, W. C. E.; Badyal, J. P. S. *Appl. Surf. Sci.* **2009**, *256*, S30–S34. (b) Friedrich, J. F.; Mix, R.; Schulze, R.-D.; Meyer-Plath, A.; Joshi, R.; Wettmarshausen, S. *Plasma Processes Polym.* **2008**, *5*, 407–423. (c) Wettmarshausen, S.; Kühn, G.; Hidde, G.; Mittmann, H.-U.; Friedrich, J. F. *Plasma Processes Polym.* **2007**, *4*, 832–839. (d) Friedrich, J.; Wettmarshausen, S.; Hennecke, M. *Surf. Coat. Technol.* **2009**, *203*, 3647–3655. (e) Teare, D. O. H.; Barwick, D. C.; Schofield, W. C. E.; Garrod, R. P.; Ward, L. J.; Badyal, J. P. S. *Langmuir* **2005**, *21*, 11425–11430. (f) Csernica, J.; Rhodes, B. D. *J. Polym. Eng.* **1999**, *19*, 1. (g) Wang, J.-H.; Chen, X.; Chen, J.-J.; Calderon, J. G.; Timmons, R. B. *Plasma Polym.* **1997**, *2*, 245–260. (h) Kiss, E.; Samu, J.; Toth, A.; Bertoti, I. *Langmuir* **1996**, *12*, 1651–1657. (i) Csernica, J.; Rince, M. *Polymer* **1993**, *34*, 2670.

(19) (a) Chen, R. T.; Muir, B. W.; Such, G. K.; Postma, A.; Evans, R. A.; Pereira, S. M.; McLean, K. M.; Caruso, F. *Langmuir* **2009**, *26*, 3388–3393. (b) Chen, R. T.; Muir, B. W.; Such, G. K.; Postma, A.; McLean, K. M.; Caruso, F. *Chem. Commun.* **2010**, *46*, 5121–5123.

(20) (a) Ade, H.; Stoll, H. *Nat. Mater.* **2009**, *8*, 281–290. (b) Retzko, I.; Friedrich, J. F.; Lippitz, A.; Unger, W. E. S. *J. Electron Spectrosc. Relat. Phenom.* **2001**, *121*, 111–129. (c) Oran, U.; Swaraj, S.; Lippitz, A.; Unger, W. E. S. *Plasma Processes Polym.* **2006**, *3*, 288–298. (d) Swaraj, S.; Oran, U.; Lippitz, A.; Schulze, R.-D.; Friedrich, J. F.; Unger, W. E. S. *Plasma Processes Polym.* **2004**, *1*, 134–140. (e) Girard-Lauriault, P.-L.; Desjardins, P.; Unger, W. E. S.; Lippitz, A.; Wertheimer, M. R. *Plasma Processes Polym.* **2008**, *5*, 631–644. (f) Johnston, E. E.; Ratner, B. D. *J. Electron Spectrosc. Relat. Phenom.* **1996**, *81*, 303–317. (g) Friedrich, J. F.; Geng, S.; Unger, W.; Lippitz, A.; Erdmann, J.; Gorsler, H. V.; Woll, C.; Schertel, A.; Bierbaum, K. *Surf. Coat. Technol.* **1995**, *74*−*75*, 664–669. (f) Swaraj, S.; Oran, U.; Lippitz, A.; Unger, W. E. S. *Plasma Processes Polym.* **2008**, *5*, 92–104.

(21) Griesser, H. J. *Vacuum* **1989**, *39*, 485–488.

(22) Beamson, G.; Briggs, H. *High Resolution XPS of Organic Polymers: The Scienta ESCA300 Database*; John Wiley & Sons: Chichester, 1992.

(23) Cowie, B. C. C.; Tadich, A.; Thomsen, L. *AIP Conf. Proc.* **2010**, *1234*, 307–310.

(24) Watts, B.; Thomsen, L.; Dastoor, P. C. *J. Electron Spectrosc. Relat. Phenom.* **2006**, *151*, 105–120.

(25) Leggett, G. J.; Ratner, B. D.; Vickerman, J. C. *Surf. Interface Anal.* **1995**, *23*, 22–28.

(26) Balamurugan, S.; Mandale, A. B.; Badrinarayanan, S.; Vernekar, S. P. *Polymer* **2001**, *42*, 2501–2512.

(27) Beck, A. J.; Candan, S.; France, R. M.; Jones, F. R.; Short, R. D. *Plasmas Polym.* **1998**, *3*, 97–114.

(28) Mähl, S.; Lachnitt, J.; Niemann, R.; Neumann, M.; Baalmann, A.; Kruse, A.; Schlett, V. *Surf. Interface Anal.* **1996**, *24*, 405–410.

(29) Huang, N. K.; Wang, D. Z.; Xiong, Q.; Yang, B. *Nucl. Instrum. Methods Phys. Res., Sect. B* **2003**, *207*, 395–401.

(30) (a) Stöhr, J. *NEXAFS Spectroscopy*; Springer: Berlin, 1992. (b) Dhez, O.; Ade, H.; Urquhart, S. G. *J. Electron Spectrosc. Relat. Phenom.* **2003**, *128*, 85–96.

(31) (a) Yasuda, H.; Bumgarner, M. O.; Hillman, J. J. *J. Appl. Polym. Sci.* **1975**, *19*, 531–543. (b) Yasuda, H.; Lamaze, C. E. *J. Appl. Polym. Sci.* **1973**, *17*, 1533–1544.

(32) (a) Shard, A. G.; Whittle, J. D.; Beck, A. J.; Brookes, P. N.; Bullett, N. A.; Talib, R. A.; Mistry, A.; Barton, D.; McArthur, S. L. *J. Phys. Chem. B* **2004**, *108*, 12472–12480. (b) Beck, A. J.; Whittle, J. D.; Bullett, N. A.; Eves, P.; Mac Neil, S.; McArthur, S. L.; Shard, A. G. *Plasma Processes Polym.* **2005**, *2*, 641–649.

(33) Urquhart, S. G.; Ade, H. *J. Phys. Chem. B* **2002**, *106*, 8531–8538.

(34) Ade, H.; Hitchcock, A. P. *Polymer* **2008**, *49*, 643–675.

(35) (a) Graf, N.; Yegen, E.; Gross, T.; Lippitz, A.; Weigel, W.; Krakert, S.; Terfort, A.; Unger, W. E. S. *Surf. Sci.* **2009**, *603*, 2849–2860. (b) Kikuma, J.; Warwick, T.; Shin, H. J.; Zhang, J.; Tonner, B. P. *J. Electron Spectrosc. Relat. Phenom.* **1998**, *94*, 271–278.

(36) Parent, P.; Laffon, C.; Tourillon, G.; Cassuto, A. *J. Phys. Chem.* **1995**, *99*, 5058–5066.